Modeling of firn compaction for estimating ice-sheet mass change from observed ice-sheet elevation change

Jun LI,[1] H. Jay ZWALLY[2]

[1]*SGT Inc., NASA Goddard Space Flight Center, Code 614.1, Greenbelt, MD 20771, USA*
E-mail: Jun.Li@nasa.gov
[2]*Cryospheric Sciences Branch, NASA Goddard Space Flight Center, Code 614.1, Greenbelt, MD 20771, USA*

ABSTRACT. Changes in ice-sheet surface elevation are caused by a combination of ice-dynamic imbalance, ablation, temporal variations in accumulation rate, firn compaction and underlying bedrock motion. Thus, deriving the rate of ice-sheet mass change from measured surface elevation change requires information on the rate of firn compaction and bedrock motion, which do not involve changes in mass, and requires an appropriate firn density to associate with elevation changes induced by recent accumulation rate variability. We use a 25 year record of surface temperature and a parameterization for accumulation change as a function of temperature to drive a firn compaction model. We apply this formulation to ICESat measurements of surface elevation change at three locations on the Greenland ice sheet in order to separate the accumulation-driven changes from the ice-dynamic/ablation-driven changes, and thus to derive the corresponding mass change. Our calculated densities for the accumulation-driven changes range from 410 to 610 kg m^{-3}, which along with 900 kg m^{-3} for the dynamic/ablation-driven changes gives average densities ranging from 680 to 790 kg m^{-3}. We show that using an average (or 'effective') density to convert elevation change to mass change is not valid where the accumulation and the dynamic elevation changes are of opposite sign.

INTRODUCTION

Knowledge of the mass balance of polar ice sheets is essential for understanding sea-level change. The recent assessment from the Intergovernmental Panel on Climate Change Fourth Assessment Report (IPCC, 2007) summarizes estimates of the mass change from both the Greenland and Antarctic ice sheets from 1993 to 2003 in the ranges from in balance (0 Gt a^{-1}) to a loss of 300 Gt a^{-1}, equivalent to a rate of sea-level rise of 0–0.8 mm a^{-1}. Other results from satellite and aircraft measurements of surface elevation change (dH/dt), satellite measurements of changes in gravity, and the mass input–output method are reviewed (Alley and others, 2007; Shepherd and Wingham, 2007) and tabulated in Dahl-Jensen and others (2009). A particular issue of concern for deriving mass changes (dM/dt) from observed dH/dt has been the appropriate density to use, because dH/dt is in general a combination of changes in firn thickness and solid-ice thickness, both of which have different densities. Recently Zwally and others (2011) reported a net mass loss from the Greenland ice sheet of 171 $\pm$ 4 Gt a^{-1} for the period 2003–07 and a loss of 7 $\pm$ 3 Gt a^{-1} for the period 1992–2002 based on dH/dt observations over these time periods. The methods for these calculations are described in more detail in this paper.

The relation between dH/dt and dM/dt is the result of multiple processes occurring throughout the ice-sheet column. For example, variations in surface air temperature cause a change in the rate of compaction in the upper firn layers, which causes a surface elevation change, but this temperature-driven change does not involve any mass change (Zwally and Li, 2002). Arthern and Wingham (1998) evaluated the impact of changes in accumulation rate, temperature and surface snow density by using a firn compaction model. Their results suggested that accumulation-rate induced changes were the most significant, and that temperature effects were relatively small. In contrast, the firn compaction model of Zwally and Li (2002) showed a larger temperature sensitivity due to their introduction of a temperature-dependent activation energy and rate coefficient based on laboratory experiments. Their results showed that the seasonal variation in surface temperature caused seasonal variations in surface elevation, as well as longer-term changes from year-to-year trends in temperature. This strong dependence of firn compaction rate on temperature has since been supported by field observations of compaction rates (Arthern and others, 2010).

Prior to Zwally and others (2011), a constant effective density, ρ_{eff}, with values between 300 and 900 kg m^{-3} was generally used to convert dH/dt to dM/dt (e.g. 350 in Davis and others, 2005; 300 for the 'interior' and 900 to 'seaward' in Thomas and others, 2006; 350 and 917 in Wingham and others, 2006). However, Figure 1 shows a case in which using a constant density is clearly not valid. Consider a location where the accumulation rate, $A(t)$, is increasing in time while the ice sheet is dynamically thinning (i.e. the firn thickness change $\mathrm{d}I_{\text{firn}}/\mathrm{d}t > 0$, and the underlying ice thickness change $\mathrm{d}I_{\text{ice}}/\mathrm{d}t < 0$, with example values of firn and ice thickness changes and associated densities given in Figure 1. The net mass change (per unit area and time) is $\mathrm{d}M/\mathrm{d}t = 200 - 900 = -700$ kg m^{-2} a^{-1}, and the net thickness change is $\mathrm{d}I/\mathrm{d}t = 0.4 - 1.0 = -0.6$ m a^{-1}. Thus, the effective density using this dI/dt would be $\rho_{\text{eff}} = (\mathrm{d}M/\mathrm{d}t)/(\mathrm{d}I/\mathrm{d}t) = -700/-0.60 = 1167$ kg m^{-3}, which is greater than the density of glacier ice, $\rho_{\text{i}} = 900$ kg m^{-3}.

Our example clearly shows that the assumption that some value of ρ_{eff} between 300 and 900 kg m^{-3} can be chosen is not always valid. In fact, it will be invalid wherever there is a combination of accumulation-driven thickening and dynamic thinning, or vice versa. Furthermore, where $\mathrm{d}I_{\text{firn}}/\mathrm{d}t = \mathrm{d}I_{\text{ice}}/\mathrm{d}t$, the corresponding value of ρ_{eff} will become infinite. This example demonstrates the necessity of estimating changes in firn thickness and ice thickness separately, and of using the appropriate densities for each.

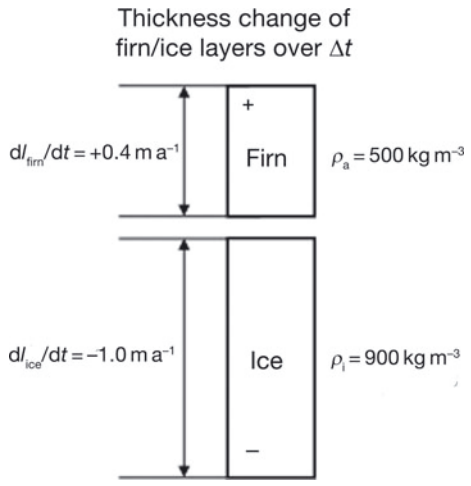

Fig. 1. Example of upper firn and deep ice thickness changes and associated mass changes, where 200 kg m^{-2} a^{-1} of firn is added to the firn–ice column by an accumulation increase and 900 kg m^{-2} a^{-1} is subtracted by dynamic thinning. In this case, the conventionally defined effective density, $\rho_{\text{eff}} = (\mathrm{d}M/\mathrm{d}t)/(\mathrm{d}l/\mathrm{d}t)$, is 1167 kg m^{-3}, which would be unrealistically greater than the density of ice.

In this paper, we present a firn compaction model for calculating changes in the rate of firn compaction caused by changes in both accumulation rate and temperature. The model is used to separate the accumulation-driven and ablation-dynamic-driven changes in surface elevation, and to calculate the appropriate firn density for accumulation-driven changes. It incorporates the processes of surface melting, percolation and refreezing. It also includes a critical improvement to accommodate a time-dependent accumulation rate, $A(t)$. We apply the method to three selected field locations in Greenland.

THE FIRN COMPACTION MODEL

As described in Zwally and Li (2002), the $\mathrm{d}H/\mathrm{d}t$ of an ice sheet is composed of several vertical-velocity components:

$$\frac{\mathrm{d}H(t)}{\mathrm{d}t} = \frac{A(t)}{\rho_{\text{sf}}} - V_{\text{fc}}(t) - \frac{A_{\text{b}}(t)}{\rho_{\text{i}}} - V_{\text{ice}} + \frac{\mathrm{d}B}{\mathrm{d}t}. \qquad (1)$$

Here accumulation rate, $A(t)$, is the component that raises the surface at a rate of $A(t)/\rho_{\text{sf}}$, where ρ_{sf} is the density of the surface snow. In general, ρ_{sf} has a value of ~330 kg m^{-3} in dry snow regions (Paterson, 1994). In areas with surface melt, the meltwater percolates downward in the firn layers and the density and thickness of firn layers are modified by the meltwater and refreezing (Li and others, 2007; Reeh, 2008). The melting and refreezing process has been incorporated in our model and is described in detail by Li and others (2007). $A_{\text{b}}(t)$ is the ablation rate occurring only in the ablation zone, V_{ice} is the vertical velocity of the ice at the firn/ice transition, and $\mathrm{d}B/\mathrm{d}t$ is the vertical motion of the underlying bedrock. $V_{\text{fc}}(t)$ is the velocity of firn compaction at the surface, which is the integral of the compressive displacement of the firn layers over the length of the firn column. Following the normal usage that surface elevation, H, is positive upwards and depth, z, is positive downwards, $\mathrm{d}H/\mathrm{d}t$, A and $\mathrm{d}B/\mathrm{d}t$ are positive upwards and V_{fc}, A_{b} and V_{ice} are positive downwards in Equation (1). According to the mass conservation equation (Li and Zwally, 2002), the velocity of firn compaction, V_{fc}, at depth z is given by the density, $\rho(z)$, and compaction rate, $\mathrm{d}\rho(z)/\mathrm{d}t$, as

$$V_{\text{fc}}(z,t) = \int_{z_{\text{i}}}^{z} \frac{1}{\rho(z)} \left[\frac{\mathrm{d}\rho(z)}{\mathrm{d}t}\right] \mathrm{d}z, \qquad (2)$$

where z_{i} is the firn–ice transition depth at which the density is ~900 kg m^{-3}.

Essential to the compaction model is the constitutive relation between the compaction rate, $\mathrm{d}\rho/\mathrm{d}t$, and the physical variables such as accumulation rate, $A(t)$, and firn temperature, $T(t)$, that drive the density change. This relation is given by

$$\frac{\mathrm{d}\rho(z)}{\mathrm{d}t} = K\big[T(z)\big]\overline{A}\big[\rho_{\text{i}} - \rho(z)\big]. \qquad (3)$$

Equation (3) is a semi-empirical relation modified from that initially proposed by Herron and Langway (1980) for the steady-state case, and $\overline{A} = \overline{A}(t)$ is the constant accumulation rate in their relation. As discussed by Zwally and Li (2002), Equation (3) is based on the idea that the compaction rate at depth z is determined by changes in overburden pressure, firn temperature and density. However, Equation (3) is not time-dependent with respect to $A(t)$ at the surface. Therefore $\overline{A}$ in Equation (3) cannot simply be replaced by $A(t)$ at $z = 0$. For example, when $A(t)$ at the surface of the ice sheet is zero, the compaction of deeper firn layers continues, but Equation (3) would indicate that the compaction rate is zero at all depths. Since $\overline{A}$ at least in part reflects the changes of overburden pressure, we replace $\overline{A}$ by the integral from the surface to depth z of $A(t-\Delta t)/\Delta t$ to represent the average change of the overburden pressure at depth z, where Δt is the time taken for the layer to propagate from the surface to depth z.

The temperature dependence of the compaction rate, $\mathrm{d}\rho(z)/\mathrm{d}t$, in Equation (3) has been conventionally taken as following an Arrhenius relation, i.e.

$$K(T) = K_0 \mathrm{e}^{-E/(RT)}, \qquad (4)$$

where $K(T)$ is the rate factor due to the temperature T in kelvin. K_0 is a constant, E is the activation energy and R is a gas constant. Experimental results of grain growth and ice creep show that the temperature dependence of $K(T)$ is more sensitive than Equation (4) under constant K_0 and E, indicating that E is actually a function of temperature, $E(T)$. Its value increases with temperature (Jacka and Li, 1994). Since both grain growth and ice creep are involved in firn compaction, Zwally and Li (2002) applied the experimental results to their firn compaction model. They indicated that an increasing value of $E(T)$ will decrease $K(T)$ if K_0 is kept constant, which is contrary to the experimental data. Therefore K_0 must also be a function of temperature, $K_0(T)$. They modified Equation (4) for firn compaction by introducing a temperature-dependent activation energy, $E(T)$, and a rate constant, $K_0(T)$, with an adjustable parameter, β, i.e.

$$K(T) = \beta K_{\text{G}}(T). \qquad (5)$$

The second term on the right-hand side in Equation (5) is the grain growth rate,

$$K_{\text{G}}(T) = K_{0\text{G}}(T)\mathrm{e}^{-E(T)/(RT)}, \qquad (6)$$

given by the experiments (Fig. 2a).

An error in the text of the Zwally and Li (2002) paper caused confusion in the application of the theory. By using a best fit to the experimental data given by Jacka and Li (1994), Zwally and Li (2002) derived the empirical expressions of grain growth rate, $K_{\text{G}}(T)$, and the activation energy,

$E(T)$, as functions of temperature, T (Fig. 2a and b). Both functions were initially given by Zwally and Li (2002, fig. 3a and b). However, K_G was mislabeled as K_{0G}. Rearranging Equation (6) we have

$$K_{0G}(T) = K_G(T)e^{E(T)/(RT)}. \quad (7)$$

Figure 2c gives the empirical form of $K_{0G}(T)$ as a function of temperature by substituting the expressions of $E(T)$ and $K_G(T)$ shown in Figure 2a and b into Equation (6), together with the function of $E(T)$. As shown by Figure 2c, K_{0G} increases with temperature apparently faster than $E(T)$, indicating the stronger temperature dependence of $K_{0G}(T)$ compared to $E(T)$. Combining Equations (4–6), we then have

$$K(T) = \beta 8.36(273.2 - T)^{-2.061}, \quad (8)$$

where β is an adjustable parameter determined by fitting modeled density profiles to field measurements. Equation (8) accounts for the temperature dependence of grain growth and ice creep rates on firn compaction. It leads to much higher temperature sensitivity than Equation (4) under constant values of K_0 and E (e.g. Herron and Langway, 1980), particularly for temperatures higher than –10°C. Equations (1–8) are coupled with a one-dimensional heat-conducting equation and solved using the multilayer system described by Zwally and Li (2002).

The empirical parameter, β, in Equation (5) is used to calibrate modeled density profiles to field measurements. In our previous version of the model, we presented β as a function of the annual mean temperature based on field density profiles from Greenland (Li and others, 2003). Helsen and others (2008) extended this relation by using 41 observed pore close-off depths (depth of the 830 kg m^{-3} density) from Antarctica where firn temperatures are much colder. They found a slightly different relation between β and the annual mean temperature. However, for temperatures higher than about –30°C (e.g. Greenland), the two relations are similar. To further improve the calibration, we use two critical points at densities of 550 and 830 kg m^{-3} as the control, and tune the value of β to force the modeled ages at these two densities to match those given by Herron and Langway (1980) that were well constrained by the field density measurements. Although the previous calibrations (Li and others, 2003; Helsen and others, 2008) showed that β is a function of annual mean temperature only, our tests indicate that the accumulation rate also had an influence, similar to the Herron and Langway (1980) density–age relation for which both temperature and accumulation rate were involved. Our present values of β as a function of annual mean temperature, T_m (°C), and long-term accumulation rate, $\langle A\rangle$ (m a^{-1}), for Greenland are

$$\begin{aligned}\beta &= \beta 1\\ &= -9.788 + 8.996\langle A\rangle - 0.6165T_m,\\ &\rho \le 550\,\text{kg m}^{-3}\end{aligned} \quad (9)$$

$$\begin{aligned}\beta &= \beta 2\\ &= \beta 1/(-2.0178 + 8.4043\langle A\rangle - 0.0932T_m),\\ &\rho > 550\ \text{kg m}^{-3}.\end{aligned} \quad (10)$$

Equations (9) and (10) produce modeled density–depth (age) profiles that are in agreement with those from Herron and Langway (1980) within an error <±1%.

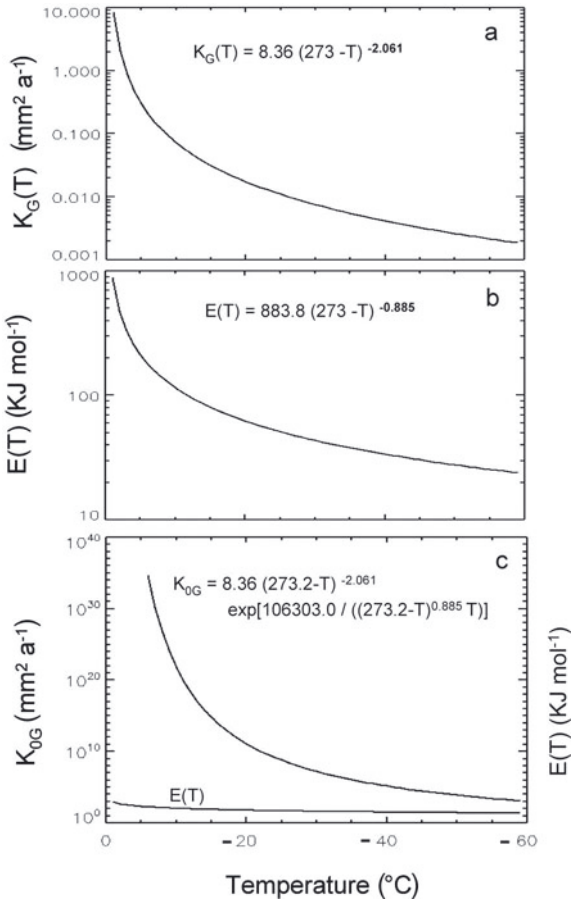

Fig. 2. (a) The temperature dependence of grain growth rate, K_G; (b) activation energy, $E(T)$, for grain growth; and (c) the derived rate constant, K_{0G}, for grain growth as a function of temperature, according to Equation (6) (shown together with $E(T)$ for comparison). Note that the empirical functions in (a) and (b) were initially given by Zwally and Li (2002, figs 3b and a). However, K_G was mislabeled as K_{0G} in their figure 3b.

ELEVATION CHANGE COMPONENTS FROM ALTIMETRY $\mathbf{d}H/\mathbf{d}t$

As described in Equation (1), the surface elevation change, dH/dt, is due to a combination of vertical velocity components from different processes. For non-steady state, these components can be represented by perturbations from steady state, assuming that dB/dt is constant during the measurements:

$$\frac{dH}{dt} = \frac{dH^a}{dt} + \frac{dC_{AT}}{dt} + \frac{dH_d}{dt} + \frac{dH_b}{dt} + \frac{dB}{dt}, \quad (11)$$

where $dH^a/dt = (A(t) - \langle A\rangle)/\rho_{sf}$ is the direct change caused by $A(t)$, $dC_{AT}/dt = -(V_{fc}(t) - \langle V_{fc}\rangle)$ is the firn compaction-rate caused elevation change driven by both $A(t)$ and $T(t)$, $dH_b/dt = -(A_b(t) - \langle A_b\rangle)/\rho_i$ is driven by changes in the ablation rate, and $dH_d/dt = -(V_{ice}(t) - \langle V_{ice}\rangle)$ is driven by dynamic changes in the ice flow relative to $\langle A\rangle$. The $\langle\rangle$ symbol indicates long-term averages of the various components, obtained during our model spin-up to a steady state. We consider that ablation is zero in the accumulation zone where firn exists. In the ablation zone where there is no firn, accumulation is zero. In general, dC_{AT}/dt depends on the history of both $A(t)$ and $T(t)$ as their effects propagate

into the firn. We separate their effects by assuming

$$\frac{dC_{AT}}{dt} = \frac{dC_A}{dt} + \frac{dC_T}{dt},$$

where dC_A/dt and dC_T/dt are changes driven by $A(t)$ and $T(t)$, respectively. The total elevation change from both $A(t)$ and $T(t)$ perturbations becomes

$$\frac{dH^a{}_{CAT}}{dt} \equiv \frac{dH^a}{dt} + \frac{dC_A}{dt} + \frac{dC_T}{dt} = \frac{dH^a{}_{CA}}{dt} + \frac{dC_T}{dt},$$

where $dH^a{}_{CA}/dt$ is the total change caused by $A(t)$, including both the direct change and that associated with the compaction rate. Equation (11) then gives

$$\frac{dI}{dt} \equiv \frac{dH}{dt} - \frac{dC_T}{dt} - \frac{dB}{dt} = \frac{dH^a{}_{CA}}{dt} + \frac{dH_{bd}}{dt}, \qquad (12)$$

where dI/dt is the net thickness change in the firn/ice column, defined by treating dB/dt and dCT/dt as corrections to dH/dt. dH_{bd}/dt is the combined ablation and dynamic term (as $dH_{bd}/dt \equiv dH_d/dt + dH_b/dt$). In the ablation zone where there is no firn, dH_{bd}/dt is the mixed term of both dynamics and melting (ablation). In the accumulation zone, dH_{bd}/dt is only the dynamic term. The two terms on the right-hand side in Equation (12) involve change in mass. To obtain $dH^a{}_{CA}/dt$, our compaction model first calculates $dH^a{}_{CAT}/dt$ using both $T(t)$ and $A(t)$, and then calculates dC_T/dt using $T(t)$ with constant $\langle A\rangle$. The $dH^a{}_{CA}/dt$ is then given by

$$\frac{dH^a{}_{CA}}{dt} = \frac{dH^a{}_{CAT}}{dt} - \frac{dC_T}{dt},$$

i.e. the total accumulation-driven change in surface elevation is obtained by subtracting the temperature-driven compaction from that caused directly by the change in accumulation rate and by the change in compaction rate driven by both accumulation and temperature variations.

MASS CHANGE FROM dH/dt COMPONENTS

Applying appropriate densities to Equation (12) on the right-hand side, the mass change rate, dM/dt, of the ice sheet is given by

$$\frac{dM}{dt}\left(\mathrm{kg\,m^{-2}\,a^{-1}}\right) = \frac{\rho_a dH^a{}_{CA}}{dt} + 900\frac{H_{bd}}{dt}. \qquad (13)$$

The appropriate density associated with the dynamic and ablation term, dH_{bd}/dt ($\mathrm{m\,a^{-1}}$), is the density of glacier ice ($900\,\mathrm{kg\,m^{-3}}$). The density, ρ_a ($\mathrm{kg\,m^{-3}}$), associated with the shorter-term change of $dH^a{}_{CA}/dt$ ($\mathrm{m\,a^{-1}}$) is discussed in the next section. In terms of dI/dt ($\mathrm{m\,a^{-1}}$), Equation (13) can be written as

$$\frac{dM}{dt} = \frac{900dI}{dt} - (900 - \rho_a)\frac{dH^a{}_{CA}}{dt}. \qquad (14)$$

Equation (14) is used to calculate the mass change of the ice sheet. It requires the altimetry measurements of dH/dt, surface temperature $T(t)$ and accumulation rate $A(t)$ histories as inputs to the compaction model to obtain dC_T/dt, $dH^a{}_{CA}/dt$ and the density, ρ_a. Equation (14) indicates that using dI/dt with the density of ice to derive dM/dt is an approximation that neglects the effects of recent changes in accumulation rate on the rate of firn compaction.

DERIVING DENSITY, ρ_a, FOR dH^a_{ca}/dt

The density, ρ_a, associated with $dH^a{}_{CA}/dt$ shown in Equations (13) and (14) is the average density caused by perturbations to the accumulation rate over a specified time period. Considering the surface elevation change driven by variations in accumulation rate $A(t)$ only, i.e. $dH/dt = dH^a{}_{CA}/dt$, the corresponding mass change, $\Delta M_a(t)$, over $\Delta t = t - t_0$ is given by

$$\Delta M_a(t) = \int_{t_0}^{t} \left[A(t) - \langle A\rangle\right] dt.$$

Here $A(t)$ and $\langle A\rangle$ are in units of $\mathrm{kg\,m^{-2}\,a^{-1}}$. $\Delta M_a(t)$ is in $\mathrm{kg\,m^{-2}}$. This mass change causes a surface elevation change of

$$\Delta H^a{}_{CA}(t) = \int_{t_0}^{t} \left(\frac{dH^a{}_{CA}}{dt}\right) dt.$$

Thus,

$$\rho_a(t) = \frac{\Delta M_a}{\Delta H^a{}_{CA}} = \int_{t_0}^{t} \left[A(t) - \langle A\rangle\right] dt \Big/ \int_{t_0}^{t} \left(\frac{dH^a{}_{CA}}{dt}\right) dt. \qquad (15)$$

Equation (15) defines the density, ρ_a, that is obtained using the firn compaction model. It represents the density of the firn that has been added (removed) as a result of an increase (decrease) in $A(t)$ relative to the density profile for the long-term average $\langle A\rangle$. However, the corresponding change in the amount of firn and the compaction rate is distributed throughout the firn column, so there is no associated physical layer in the firn with a density ρ_a and thickness $dH^a{}_{CA}/dt$.

RESULTS AND DISCUSSION

The appropriate method to derive the mass change, dM/dt, is described by Equation (14). Here we derive the values at three selected locations on the Greenland ice sheet (Fig. 3). Site A is in the northern region and is associated with lower accumulation rate and temperature. Site B is near the Summit of the ice sheet, and site C, in the south, is associated with much higher accumulation rate and temperature. We use monthly surface temperatures, $T_s(t)$, for January 1982–October 2007 as shown in Figure 4a from the Advanced Very High Resolution Radiometer (AVHRR) (Comiso, 2003). We parameterize changes in the accumulation rate, $A(t)$, according to the annual mean surface temperature at the rate of $5\%\,\mathrm{K^{-1}}$. The IPCC report (IPCC, 2007) summarized the sensitivity of accumulation rate to temperature with a range 4.7–8.5% $\mathrm{K^{-1}}$. Data from Greenland ice cores (Clausen and others, 1988) give a range 4–6% $\mathrm{K^{-1}}$ based on a sensitivity of $\delta^{18}O$ to temperature of $0.69‰\,\delta^{18}O\,\mathrm{K^{-1}}$ (Zwally and Giovinetto, 1997). For 1988–2005, this parameterization gives an average $A(t)$ increase of $0.6\%\,\mathrm{a^{-1}}$. This is close to the $0.7\%\,\mathrm{a^{-1}}$ for 1988–2004 inferred from a regional-climate and surface mass-balance model for the percolation and dry-snow zones of Greenland (Box and others, 2006). Although there is a good relation between changes in accumulation and temperature for annual mean values, the correlation could be poor for short-term changes (Kapsner and others, 1995). Therefore, in our $A(t)$ parameterization, we use the annual mean temperatures instead of monthly temperatures to avoid introducing seasonal variations in $A(t)$ due to strong seasonal variations in temperature. A more sophisticated approach that would

Fig. 3. A map showing three selected test locations: A (79.4° N, 319.9° E), B (72.9° N, 321.2° E) and C (61.9° N, 315.9° E) on the Greenland ice sheet. The climatic characteristics for the three locations are given in Table 1.

avoid some of these complications in the sensitivity between temperature and accumulation rate would be to use $A(t)$ from the climate models (e.g. Helsen and others, 2008).

Starting from the initial steady-state spin-up, we applied the time series of $T_s(t)$ and $A(t)$ to our compaction model. Figure 4c shows the modeled time variations in the three components from firn compaction at site B, driven by the variations in $T_s(t)$ and $A(t)$ shown in Figure 4a and b. The profiles show significant interannual variations, especially since 2000 due to the enhanced warming in that period. Although the input temperatures are monthly mean values, the annual cycles in the temperature profile still cause seasonal variations in $C_T(t)$ and $H^a_{CAT}(t)$ profiles, but with smaller amplitudes (~2 cm) compared to the results from model runs using hourly or daily timescales (Zwally and Li, 2002). In contrast, the $H^a_{CA}(t)$ profile does not have seasonal variations, because our parameterization of $A(t)$ does not have a seasonal variation. We use best fits to the profiles in Figure 4c for site B (and the similar profiles for sites A and C), for the period October 2003–October 2007, to obtain the mass change rates, dM/dt, and associated components for the three sites as summarized in Table 1. The associated dH/dt are derived from Ice, Cloud and land Elevation Satellite (ICESat) measurements for the same period, and dB/dt were

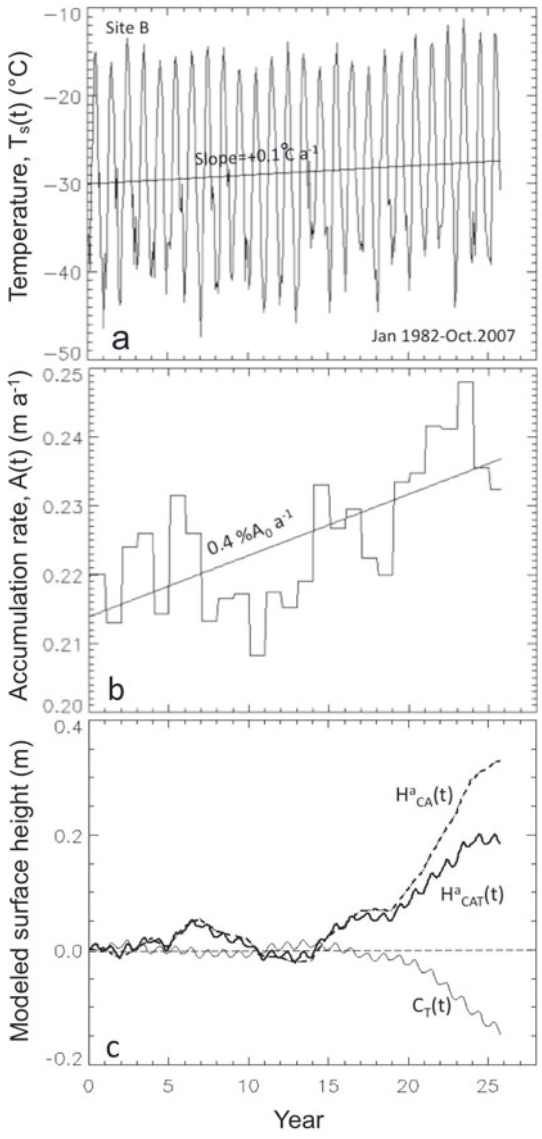

Fig. 4. (a) Mean monthly surface temperature at site B in Greenland (Fig. 3) showing the general warming during the last two decades. (b) The associated increase in accumulation rate as a function of the annual mean temperature using a rate of 5% K^{-1}. (c) The modeled surface height changes in three components (as marked) from firn compaction driven by temperature and the accumulation rate histories shown in (a) and (b).

Table 1. The climatic characteristics and the derived rates of the mass change, dM/dt, and associated values of the components of elevation change as described by Equation (14), together with other parameters for three selected locations (Fig. 3) on the Greenland ice sheet. Calculation of dM/dt requires determination of the accumulation-driven component, dH^a_{CA}/dt, and its associated density, ρ_a, and the ice-dynamic- and ablation-driven component, dH_{bd}/dt, with density of 900 kg m^{-3}, as well as correction of the observed dH/dt for temperature-driven variations in firn compaction, dC_T/dt, and bedrock motion, dB/dt

Site	$\langle A \rangle$	T_m	dH/dt	dC_T/dt	dB/dt	dI/dt	dH^a_{CA}/dt	dH_{bd}/dt	ρ_a	ρ_{avg}	ρ_{eff}	dM/dt
	m a^{-1}	°C	m a^{-1}	m a^{-1}	m a^{-1}	m a^{-1}	m a^{-1}	m a^{-1}	kg m^{-3}	kg m^{-3}	kg m^{-3}	kg m^{-2} a^{-1}
A	0.10	–29.3	0.068	–0.016	0.002	0.082	0.019	0.063	410	786	786	64.5
B	0.22	–29.7	0.046	–0.023	–0.003	0.072	0.036	0.036	460	680	680	49.0
C	0.90	–14.0	–0.083	–0.051	0.003	-0.035	0.104	–0.139	610	776	1762	–61.7

averaged from three models as in Zwally and others (2005). As shown in Table 1, the impacts from the temperature- and accumulation-driven components, dC_T/dt and dH^a_{CA}/dt, are of similar magnitudes, but the temperature increase causes a surface elevation decrease that is offset by the increase in the accumulation rate. At site C, the measured surface elevation change, dH/dt, is $-0.083\ m\ a^{-1}$ and dH^a_{CA}/dt is $0.104\ m\ a^{-1}$, indicating that the obtained mass loss ($-61.7\ kg\ m^{-2}\ a^{-1}$) is due to the ice-dynamic imbalance and/or ablation. Also, we note that for site C the values of dM/dt and dI/dt from Table 1 give a conventionally defined effective density of $1762\ kg\ m^{-3}$, which is greater than the density of ice as in the example of Figure 1.

Once the components required for dM/dt in Equation (14) are known, the average physical density can be calculated using

$$\rho_{avg} = \frac{\left(\rho_a \left|\frac{dH^a_{CA}}{dt}\right| + \rho_i \left|\frac{dH_{bd}}{dt}\right|\right)}{\left|\frac{dH^a_{CA}}{dt}\right| + \left|\frac{dH_{bd}}{dt}\right|}. \quad (16)$$

Together with Equation (12), Equation (16) describes the relationship between the net firn/ice thickness change, dI/dt, and the total thickness change ($|dH^a_{CA}/dt| + |dH_{bd}/dt|$) associated with the derived densities. When dH^a_{CA}/dt and dH_{bd}/dt have the same sign, ρ_{avg} equals ρ_{eff} ($=dM/dt/dI/dt$) and the conventional method ($dM/dt = \rho_{eff} dI/dt$) would give an arithmetically valid mass change. However, when dH^a_{CA}/dt and dH_{bd}/dt have opposite signs (e.g. Fig. 1 and Table 1 for site C), the conventional method is not valid. Equation (16) shows the importance of separating total thickness change into firn thickness change and ice thickness change. The derived ρ_{avg} for the three sites are summarized in Table 1, together with the corresponding values of ρ_{eff} for comparison. The comparison shows that ρ_{avg} is a more meaningful parameter than ρ_{eff}, but neither ρ_{avg} nor ρ_{eff} can be used to convert dI/dt or dH/dt to dM/dt.

Positive values of dH_{bd}/dt for sites A and B as shown in Table 1 indicate that the ice flow is less than required to balance the long-term average $\langle A \rangle$, which results in dynamic thickening in the same manner as negative dH_{bd}/dt results in dynamic thinning. The distribution of accumulation-driven changes and dynamic-/ablation-driven changes of the ice sheet, and changes in those parameters with time are described by Zwally and others (2011).

CONCLUSION

Altimetry-derived surface elevation changes, dH/dt, can be divided into the components driven by the variations in the following: short-term accumulation rate (i.e. dH^a_{CA}/dt), surface temperature (i.e. dC_T/dt), ice-dynamic imbalance and ablation (i.e. dH_{bd}/dt) and bedrock motion (i.e. dB/dt). Partitioning altimetry-derived surface elevation change allows assessment of the impacts from recent climate variations versus those from long-term ice-dynamic changes, leading to more accurate estimations of ice-sheet mass balance. Along with $900\ kg\ m^{-3}$ for the dynamic-/ablation-driven changes, our calculated densities for the accumulation-driven changes range from 410 to $610\ kg\ m^{-3}$, corresponding to average densities, ρ_{avg}, ranging from 680 to $790\ kg\ m^{-3}$. In the locations where thickness changes in the firn and ice layers are in opposite directions, the net thickness change as derived from the observed dH/dt cannot be transformed into mass change simply by using a constant average (or effective) density (i.e. a value between 300 and $900\ kg\ m^{-3}$).

ACKNOWLEDGEMENTS

This research was supported by NASA's ICESat Project Science funding. We thank S.F. Price and two anonymous referees for their valuable comments, which helped greatly to improve the paper.

REFERENCES

Alley, R.B., M.K. Spencer and S. Anandakrishnan. 2007. Ice-sheet mass balance: assessment, attribution and prognosis. *Ann. Glaciol.,* **46**, 1–7.

Arthern, R.J. and D.J. Wingham. 1998. The natural fluctuations of firn densification and their effect on the geodetic determination of ice sheet mass balance. *Climatic Change,* **40**(4), 605–624.

Arthern, R.J., D.G. Vaughan, A.M. Rankin, R. Mulvaney and E.R. Thomas. 2010. In situ measurements of Antarctic snow compaction compared with predictions of models. *J. Geophys. Res.,* **115**(F3), F03011. (10.1029/2009JF001306.)

Box, J.E. *and 8 others*. 2006. Greenland ice sheet surface mass balance variability (1988–2004) from calibrated polar MM5 output. *J. Climate,* **19**(12), 2783–2800.

Clausen, H.B., N.S. Gundestrup, S.J. Johnsen, R. Bindschadler and J. Zwally. 1988. Glaciological investigations in the Crête area, central Greenland: a search for a new deep-drilling site. *Ann. Glaciol.,* **10**, 10–15.

Comiso, J.C. 2003. Warming trends in the Arctic from clear satellite observations. *J. Climate,* **16**(21), 3498–3510.

Dahl-Jensen, D. *and 13 others*. 2009. *The Greenland ice sheet in a changing climate: snow, water, ice and permafrost in the Arctic*. Oslo, Arctic Monitoring and Assessment Programme.

Davis, C.H., Y. Li, J.R. McConnell, M.M. Frey and E. Hanna. 2005. Snowfall-driven growth in East Antarctic ice sheet mitigates recent sea-level rise. *Science,* **308**(5730), 1898–1901.

Helsen, M.M. *and 7 others*. 2008. Elevation changes in Antarctica mainly determined by accumulation variability. *Science,* **320**(5883), 1626–1629.

Herron, M.M. and C.C. Langway, Jr. 1980. Firn densification: an empirical model. *J. Glaciol.,* **25**(93), 373–385.

Intergovernmental Panel on Climate Change (IPCC). 2007. Summary for policymakers. In Solomon, S. *and 7 others, eds. Climate change 2007: the physical science basis. Contribution of Working Group I to the Fourth Assessment Report of the Intergovernmental Panel on Climate Change*. Cambridge, etc., Cambridge University Press, 1–24.

Jacka, T.H. and J. Li. 1994. The steady-state crystal size of deforming ice. *Ann. Glaciol.,* **20**, 13–18.

Kapsner, W.R., R.B. Alley, C.A. Shuman, S. Anandakrishnan and P.M. Grootes. 1995. Dominant influence of atmospheric circulation on snow accumulation in Greenland over the past 18,000 years. *Nature,* **373**(6509), 52–54.

Li, J. and H.J. Zwally. 2002. Modeled seasonal variations of firn density induced by steady-state surface air-temperature cycle. *Ann. Glaciol.,* **34**, 299–302.

Li, J., H.J. Zwally, H. Cornejo and D. Yi. 2003. Seasonal variation of snow-surface elevation in North Greenland as modeled and detected by satellite radar altimetry. *Ann. Glaciol.,* **37**, 233–238.

Li, J., H.J. Zwally and J.C. Comiso. 2007. Ice sheet elevation changes caused by variations of the firn compaction rate induced by satellite-observed temperature variations (1982–2003). *Ann. Glaciol.,* **46**, 8–13.

Paterson, W.S.B. 1994. *The physics of glaciers. Third edition.* Oxford, etc., Elsevier.

Reeh, N. 2008. A nonsteady-state firn-densification model for the percolation zone of a glacier. *J. Geophys. Res.,* **113**(F3), F03023. (10.1029/2007JF000746.)

Shepherd, A. and D. Wingham. 2007. Recent sea-level contributions of the Antarctic and Greenland ice sheets. *Science,* **315**(5818), 1529–1532.

Thomas, R., E. Frederick, W. Krabill, S. Manizade and C. Martin. 2006. Progressive increase in ice loss from Greenland. *Geophys. Res. Lett.,* **33**(10), L10503. (10.1029/2006GL026075.)

Wingham, D.J., A. Shepherd, A. Muir and G.J. Marshall. 2006. Mass balance of the Antarctic ice sheet. *Philos. Trans. R. Soc. London, Ser. A,* **364**(1844), 1627–1635.

Zwally, H.J. and M.B. Giovinetto. 1997. Areal distribution of the oxygen-isotope ratio in Greenland. *Ann. Glaciol.,* **25**, 208–213.

Zwally, H.J. and J. Li. 2002. Seasonal and interannual variations of firn densification and ice-sheet surface elevation at Greenland summit. *J. Glaciol.,* **48**(161), 199–207.

Zwally, H.J. *and 7 others*. 2005. Mass changes of the Greenland and Antarctic ice sheets and shelves and contributions to sea-level rise: 1992–2002. *J. Glaciol.,* **51**(175), 509–527.

Zwally, H.J. *and others*. 2011. Greenland ice sheet mass balance: distribution of increased mass loss with climate warming. *J. Glaciol.,* **57**(201), 88–102.